The Astrophysical Journal, 691:1494–1500, 2009 February 1 doi:10.1088/0004-637X/691/2/1494

A SURVEY OF C_4H, C_6H, AND C_6H^- WITH THE GREEN BANK TELESCOPE

H. Gupta[1,2,3], C. A. Gottlieb[1,2], M. C. McCarthy[1,2], and P. Thaddeus[1,2]
[1] Harvard-Smithsonian Center for Astrophysics, 60 Garden St., Cambridge, MA 02138, USA
[2] School of Engineering & Applied Sciences, Harvard University, 29 Oxford St., Cambridge, MA 02138, USA
Received 2008 August 7; accepted 2008 September 29; published 2009 February 5

ABSTRACT

A survey of the carbon chain negative ion C_6H^- and the structurally similar radicals C_4H and C_6H has been done with the 100 m Green Bank Telescope toward 24 galactic molecular sources. The most readily observed molecular anion to date, C_6H^- was detected in two new sources: the dark clouds L1544 and L1521F, where it was found to be present at the level of 2.5% ± 0.8% and 4% ± 1%, respectively relative to neutral C_6H. C_4H was detected in nearly all dark clouds surveyed (in six for the first time), and C_6H was detected in five dark clouds and one translucent cloud. The observed C_6H^-/C_6H (1%–4%) and C_6H/C_4H (0.2%–1%) ratios in these sources suggest that C_6H^- may be close to detection in many other dark clouds. The fractional ionization derived from the C_6H^-/C_6H ratio in L1544 and L1521F of 10^{-8} to 10^{-7} is comparable to earlier estimates from positive molecular ions.

Key words: ISM: molecules – molecular data – molecular processes – radio lines: ISM

1. INTRODUCTION

Negative molecular ions (anions) had long been predicted to be constituents of the interstellar gas (Dalgarno & McCray 1973; Sarre 1980; Herbst 1981), but have only been discovered recently, starting with the identification of the large carbon chain anion C_6H^- in two sources: the expanding molecular shell of the evolved carbon star IRC+10216, and the cold dark cloud TMC-1 (McCarthy et al. 2006). More recently, C_6H^- has been detected in the low-mass star forming region L1527 (Sakai et al. 2007). So far C_6H^- is the most readily detected molecular anion in astronomical sources, plausibly because C_6H is small enough to be produced at fairly high abundances in molecular clouds, but large enough for efficient electron attachment (Herbst & Osamura 2008). In the known sources of anions, lines of C_6H^- are several times stronger than those of all other molecular anions (Cernicharo et al. 2007; Brünken et al. 2007; Remijan et al. 2007; Kawaguchi et al. 2007; Thaddeus et al. 2008).

In contrast, positive molecular ions (cations) have been known to exist since the beginning of molecular astronomy, with CH^+ being one of the first three molecules identified in the interstellar gas (Douglas & Herzberg 1941). The two most widely distributed molecular cations, HCO^+ and N_2H^+, have been used to study the physical and chemical conditions in many astronomical sources (e.g., Turner & Thaddeus 1977; Womack et al. 1992; Caselli et al. 2002a).

To determine the distribution of molecular anions in space and to better establish their abundance relative to that of their neutral counterparts, a survey of C_6H^- with the 100 m Green Bank Telescope (GBT)[4] in 24 galactic molecular sources was recently undertaken. The essential purpose of this survey was to find new sources of C_6H^-, but in the process we have surveyed the related carbon chains of C_4H and C_6H as well. Here we summarize the results of this survey, including the detections of C_4H and C_6H in several new sources, and C_6H^- in two new dark clouds.

[3] Also at: Institute for Theoretical Chemistry, Departments of Chemistry and Biochemistry, The University of Texas at Austin, Austin, TX 78712, USA.
[4] The National Radio Astronomy Observatory is a facility of the National Science Foundation operated under cooperative agreement by Associated Universities, Inc.

2. OBSERVATIONS

The observations were done with the NRAO 100 m GBT (see Table 1 for specifications). The main survey consisted of simultaneous observations of lines of C_4H, C_6H, and C_6H^- between 18–22 GHz with the *K*-band receiver, but a few observations were done during poor weather between 8–10 GHz with the *X*-band receiver. In addition, a search was done for C_6H^- in two sources, Sgr B2(N) and W51 (M/S), at 13.8 GHz with the *Ku*-band receiver, but we did not search for C_6H at *Ku*-band as the observations were done prior to the identification of C_6H^-.

The observing procedure was nearly the same as that described previously (Brünken et al. 2007). Spectra were acquired by position switching, with a frequency resolution across a 50 MHz wide band in narrow line sources or a 200 MHz band in wide line sources, as summarized in Table 1. At all frequencies, two orthogonal polarizations were observed simultaneously and averaged to improve the signal-to-noise ratio.

Twenty-four sources were covered in the survey. Of these, about half are dark clouds; the rest include translucent and diffuse clouds, photon-dominated regions (PDRs), low-mass protostars, giant molecular clouds associated with H II regions, and circumstellar envelopes of carbon-rich stars (Table 2). Nine were selected because of prior evidence of C_4H and two of C_6H (see Table 2); others known to contain HC_3N and larger cyanopolyynes but not necessarily carbon chain radicals were also included.

3. RESULTS

The survey results toward dark clouds are given in Section 3.1, those toward L1544 and L1521F are described in Section 3.1.1, and trends in the abundances of carbon chains are presented in Section 3.1.2. Results for some representative molecular sources other than dark clouds are summarized in Section 3.2. The intensities, widths, and velocities of the observed lines are listed in Tables 3 and 4. Derived column densities and abundance ratios are summarized in Table 5.

3.1. Dark Clouds

Twelve dark clouds—eight in the Taurus complex—were observed in the present survey. Large carbon chain radicals had

Table 1
GBT Specifications

ν (GHz)	η	$\Delta\nu$ (kHz)	T_{sys} (K)	Date
8–10	0.94	1.5, 6.1	20–35	2008 Apr–May
12–15.4	0.92	24.4	20–35	2006 Jun
18–22.4	0.86	1.5, 6.1	30–60	2008 Apr–May
...		24.4	30–60	2008 Apr–May

Note. Beam diameter = $740/\nu$ (FWHM), η is the telescope beam efficiency, $\Delta\nu$ is the resolution, and T_{sys} is the total system temperature including contribution from the earth's atmosphere.

Table 2
Source List

Source	α(1950)	δ(1950)	Ref.
Dark Clouds:			
Barnard 1[a]	03 30 10.5	+30 57 47	1
L1495B[b]	04 12 35.3	+28 40 19	2
L1521B[a,b]	04 21 10.5	+26 30 00	2
IRAM04191+1522[a]	04 24 47.6	+15 36 36	3
L1521F[a]	04 25 35.0	+26 44 60	4
L1521E[b]	04 26 12.5	+26 07 17	5
L1551[a]	04 28 40.0	+18 01 42	6
L1512	05 00 54.4	+32 39 00	4,7
L1544[b]	05 01 12.3	+25 06 40	4
L183[b]	15 51 32.7	−02 39 30	4
L1082A[a]	20 52 20.1	+60 03 14	8
L1251[a]	22 37 51.5	+74 55 50	8
Translucent and Diffuse Clouds:			
CB17(L1389)[a,b]	04 00 36.0	+56 47 59	9,10
B0415+379 (3C111)	04 15 01.5	+37 54 07	11,12
Photon-Dominated Region:			
Horsehead Nebula[b,c]	05 38 23.4	−02 29 29	13
Low-Mass Protostars:			
NGC1333-2A	03 25 50.9	+31 04 18	14,15
NGC1333-4A	03 26 05.0	+31 03 13	14,15
Giant Molecular Clouds:			
W3 (HCN)	02 21 47.0	+61 52 54	16
Sgr B2(N)	17 44 10.0	−28 21 15	17
W51 (M/S)	19 21 26.3	+14 24 35	17
Carbon-Rich Circumstellar Envelopes:			
CRL618[b]	04 39 33.8	+36 01 15	18
CIT6	10 13 11.0	+30 49 17	18
CRL2688[b,c]	21 00 20.0	+36 29 44	18,19,20
CRL3068	23 16 42.4	+16 55 10	18

Notes. Units: right ascension in hours, minutes, and seconds; declination in degrees, arcminutes, and arcseconds.
[a]Source contains a low-mass protostellar object observed in either IRAS or *Spitzer* IR surveys.
[b]Indicates previous detection of C_4H.
[c]Previous detection of C_6H.
References. (1) Bachiller et al. 1990; (2) Hirota et al. 2004; (3) Belloche et al. 2002; (4) Crapsi et al. 2005; (5) Hirota et al. 2002; (6) Sakai et al. 2008; (7) Fuller & Myers 1993; (8) Williams et al. 1998; (9) Turner 1994; (10) Buckle et al. 2006; (11) Cox et al. 1988; (12) Lucas & Liszt 2000; (13) Teyssier et al. 2004; (14) Lefloch et al. 1998; (15) Jörgensen et al. 2005; (16) Morris et al. 1976; (17) Madden et al. 1989; (18) Fukasaku et al. 1994; (19) Highberger et al. 2001; (20) Highberger et al. 2003.

previously been observed in only a few: C_4H in 10 (five of which are covered here) and C_6H in two (TMC-1 and L1527). Here, C_4H was detected in 11 dark clouds and C_6H in five. In many of these, lines of C_4H are moderately intense ($T_A > 100$ mK), and in some, only 2–5 times weaker than those in TMC-1

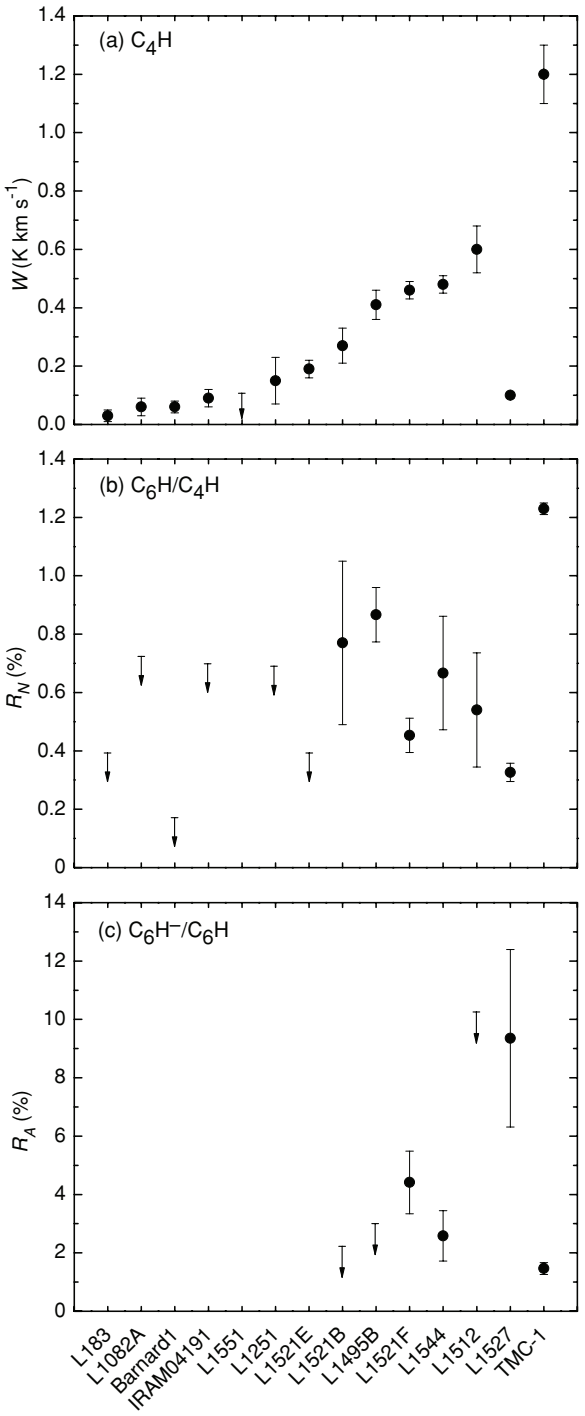

Figure 1. Comparison of C_4H, C_6H, and C_6H^- in dark clouds. (a) Velocity-integrated intensity ($W = \int T_A dv$) of the $N = 2 - 1$ lines of C_4H; data for L183 and Barnard 1 have been scaled from observations of the $N = 1 - 0$ lines, and for L1527 from the $N = 9 - 8$ lines; (b) the C_6H/C_4H ratio (R_N); and (c) the C_6H^-/C_6H ratio (R_A). Data for TMC-1 are from Brünken et al. (2007) and Thaddeus et al. (2008) and those for L1527 from Sakai et al. (2007, 2008).

(Figure 1(a)). Where C_6H is detected, its lines are only about 2–6 times weaker than those in TMC-1 and the column density is linearly related to that of C_4H (slope = 1.3 ± 0.3, correlation coefficient = 0.90).

Two sources in Taurus—L1544 and L1521F—show strong lines of C_4H and C_6H, and it is in these that the carbon chain anion C_6H^- was detected (Figures 2 and 3). The new detections double the number of dark clouds where C_6H^- is known. In a

Table 3
Observed Line Parameters

Source	C_4H				C_6H				C_6H^-			
	T_A[a]	v_{LSR}	Δv	$\int T_A dv$	T_A[b]	v_{LSR}	Δv	$\int T_A dv$	T_A	v_{LSR}	Δv	$\int T_A dv$
Dark Clouds:												
L1512	455(7)	7.14(3)	0.15(2)	0.60(8)	60(12)	7.12(3)	0.10(2)	0.04(1)	< 47	...	0.15	< 0.007
L1521B	372(11)	6.32(3)	0.17(3)	0.27(6)	40(6)	6.53(3)	0.32(5)	0.06(2)	< 14	...	0.2	< 0.003
	232(13)	6.53(3)	0.13(3)									
L1495B	590(20)	7.67(3)	0.26(3)	0.41(5)	130(20)	7.62(4)	0.23(3)	0.11(1)	< 30	...	0.25	< 0.008
L183[c]	90(10)	2.30(4)	0.26(3)	0.03(2)	< 50	...	...	< 0.015	< 63	...	0.3	< 0.019
Barnard1[c]	20(4)	6.49(4)	1.4(3)	0.06(2)	< 8	...	1.5	< 0.013	< 11	...	1.5	< 0.016
L1521E	240(20)	6.77(3)	0.26(3)	0.19(3)	< 72	...	0.3	< 0.022	< 42	...	...	< 0.013
IRAM04191+1522	90(10)	6.68(3)	0.32(5)	0.09(3)	< 60	...	0.3	< 0.02	< 40	...	0.3	< 0.014
L1082A	50(10)	2.12(7)	0.3(1)	0.06(3)	< 60	...	0.3	< 0.012	< 50	...	0.3	< 0.01
L1551	< 50	...	0.5	< 0.104	< 50	...	0.5	< 0.03	< 40	...	0.5	< 0.02
L1251	48(8)	−3.48(6)	0.7(1)	0.15(8)	< 50	...	1.0	< 0.05	< 33	...	1.0	< 0.04
Translucent and Diffuse Clouds:												
CB17(L1389)	160(10)	−4.73(3)	0.30(3)	0.15(2)	18(5)	−4.77(5)	0.30(5)	0.02(1)	< 0.023	...	0.3	< 0.007
3C111	< 14	...	2	< 0.03	< 15	...	2	< 0.03	< 11	...	2	< 0.022
Photon-Dominated Region:												
Horsehead Nebula	< 13	...	0.7	< 0.01	< 13	...	0.7	< 0.01	< 17	...	0.7	< 0.012
Low-Mass Protostars:												
NGC1333-2A	< 15	...	5	< 0.075	< 16	...	5	< 0.08	< 14	...	5	< 0.07
NGC1333-4A	< 13	...	5	< 0.065	< 18	...	5	< 0.09	< 13	...	5	< 0.065
Giant Molecular Clouds:												
W3(HCN)	< 8	...	5	< 0.04	< 12	...	5	< 0.06	< 10	...	5	< 0.05
Sgr B2(N)[d]	< 6	...	20	< 0.12								
W51 (M/S)[d]	< 7	...	15	< 0.11								
Carbon-Rich Circumstellar Envelopes:												
CRL618	< 7	...	15	< 0.11	< 12	...	15	< 0.18	< 8	...	15	< 0.12
CIT6	< 7	...	25	< 0.18	< 8	...	25	< 0.20	< 9	...	25	< 0.23
CRL2688	9(1)	−33(1)	29(2)	0.41(4)	4(1)	−33(1)	29(2)	0.11(5)	< 3	...	30	< 0.09
CRL3068	< 5	...	24	< 0.13	< 6	...	24	< 0.15	< 6	...	24	< 0.15

Notes. Units: T_A in mK, v_{LSR} and Δv in km s^{-1}, and $\int T_A dv$ in K km s^{-1}. Line parameters derived from least-squares fits of Gaussian profiles to observed spectra. For C_4H and C_6H, $\int T_A dv$ has been summed over all fine and hyperfine components. Except where noted lines were observed in the 18-22 GHz band. See Table 4 for line parameters in L1544 and L1521F.

[a]Peak intensity of the strongest hyperfine component of C_4H (N, J, $F = 2, 2.5, 3 - 1, 1.5, 2$) at 19015.144 MHz.

[b]Peak intensity of the strongest hyperfine component of C_6H ($^2\Pi_{3/2}$, $J = 6.5 - 5.5$, $F = 7 - 6$, e) at 18020.574 MHz.

[c]From observations in 8–10 GHz band. See Brünken et al. (2007) for rest frequencies.

[d]From observations in 12–15 GHz band. Rest frequency for C_6H^- is 13768.612 MHz (McCarthy et al. 2006).

few other dark clouds, where lines of C_6H are comparable in strength to those in L1544 and L1521F, C_6H^- may be close to detection (e.g., there is a hint of a weak line, about 10 mK, in L1521B after 8 hr of observation).

3.1.1. L1544 and L1521F

L1544 is one of the best known examples of a prestellar core apparently close to gravitational collapse, while L1521F has recently been found to contain a faint protostar (Crapsi et al. 2005, Bourke et al. 2006). Single antenna and interferometric observations of N_2H^+, N_2D^+, $C^{18}O$, CS, and CCS and millimeter-wave dust continuum observations toward both sources reveal several features associated with the earliest stages of low-mass star formation: (1) a high degree of CO depletion; (2) dense (10^6 cm^{-3}) cores surrounded by extended lower density ($\sim 10^4$–10^5 cm^{-3}) gas; (3) evidence for gravitational infall from the widths and asymmetric velocity profiles of molecular lines; and (4) enhanced deuterium fractionation as indicated by the large N_2D^+/N_2H^+ ratio (Tafalla et al. 1998; Ohashi et al. 1999; Caselli et al. 2002b, 2002c; Crapsi et al. 2004, 2005).

Double-peaked line profiles of C_4H, C_6H, and C_6H^- were detected toward the peak N_2D^+ emission in L1544. The partially resolved peaks are quite narrow,[5] with a weak component at 7.1 km s^{-1} and a stronger one at 7.35 km s^{-1} (Figure 2). The observed doubling is not hyperfine structure, because the separation between the two components ($\sim$ 0.25 km s^{-1}) is much smaller than the hyperfine splitting in C_4H and C_6H (see Figure 2 and Table 4), and because fine and hyperfine structure is absent in the closed-shell C_6H^- (McCarthy et al. 2006). The relative intensities of the two velocity components are reversed with respect to those of other molecular lines (e.g., N_2D^+ and N_2H^+; Caselli et al. 2002b). Because the lines of all three carbon chains are probably optically thin, the observed asymmetry is unlikely to result from self-absorption; it is more likely caused by a spatial asymmetry in the source, with more redshifted than blueshifted gas, the dip in the center resulting from freeze-out of long carbon chains in the core of L1544 (P.C. Myers 2008, private communication).

C_4H, C_6H, and C_6H^- were also detected near the peak emission of N_2D^+ in L1521F (Figure 3). As shown in the left-hand panel of Figure 3, the line profiles of C_4H, C_6H, and C_6H^- are asymmetric, but do not show well-resolved velocity structure

[5] The observed line widths are only about 1.5–2 times larger than the thermal line width of 0.1 km s^{-1} (FWHM) at 10 K.

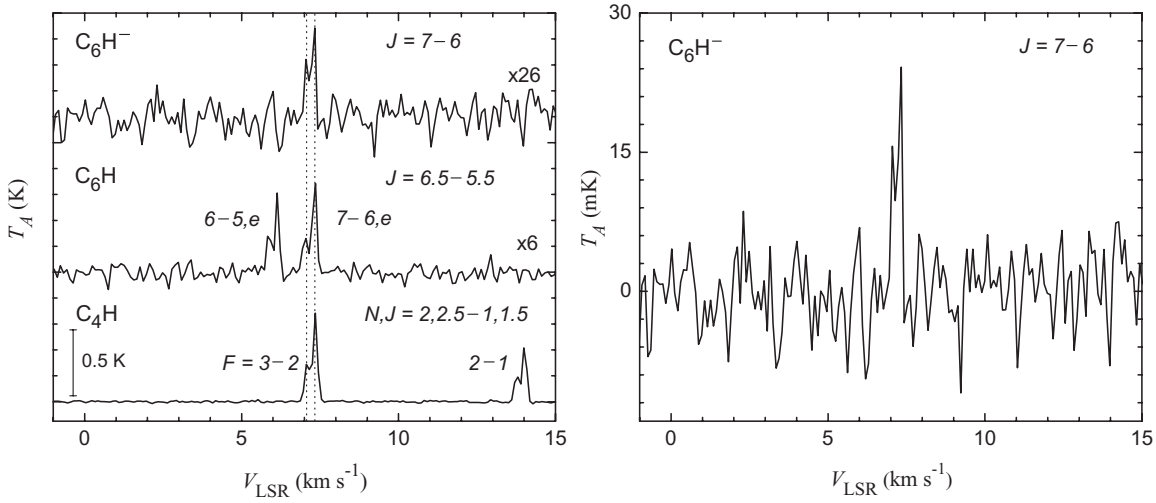

Figure 2. Line profiles of C_6H^-, C_6H, and C_6H toward L1544. Left: Spectra of C_6H^-, C_6H, and C_4H showing similar velocity structure in all three species. Lines of C_6H^- and C_6H have been scaled to the peak intensity of the C_4H line; the dashed lines are at velocities of 7.1 and 7.35 km s^{-1}. Right: Blow-up of C_6H^-. Spectra are smoothed to a resolution of 6.1 kHz. The total integration time is 10 hr for C_6H^-, and 4 hr for C_6H and C_4H.

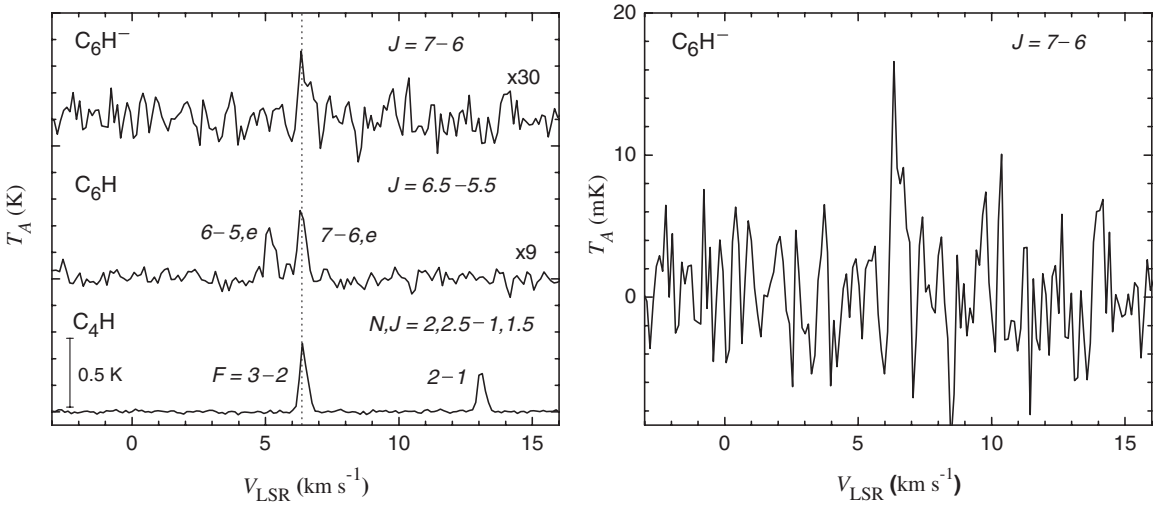

Figure 3. Line profiles of C_6H^-, C_6H, and C_6H in L1521F. Left: Spectra of C_6H^-, C_6H, and C_4H showing unresolved asymmetric lines, which peak at a velocity of 6.4 km s^{-1} (dashed line). Lines of C_6H^- and C_6H have been scaled to the peak intensity of the C_4H line. Right: Blow-up of C_6H^-. Spectra are smoothed to a resolution of 7.5 kHz. The total integration time is 10 hr for lines of C_6H^- and C_6H and 2 hr for C_4H.

like that toward L1544, possibly because of the more complex structure of this source (Crapsi et al. 2004). The asymmetric profiles observed here are similar to those found for HC_5N (Codella et al. 1997).

3.1.2. Relative Abundances of Carbon Chains

For simplicity, we define R_N as the C_6H/C_4H ratio and R_A as C_6H^-/C_6H. Five trends are apparent in the dark clouds surveyed here: (1) the column densities of C_6H and C_4H are strongly correlated; (2) R_N lies approximately between that observed in L1527 and TMC-1 (0.2%–1%; Figure 1(b)); (3) R_A is similar to that in TMC-1 and L1527 (1%–10%; Figure 1(c)); (4) R_N approaches that in TMC-1 in only two sources (L1495B and L1521B); and (v) R_A does not exceed that of L1527. The highest observed R_N is in L1495B and R_A in L1521F; the lowest observed R_N is in L1521F and R_A in L1544.

3.2. Other sources

In sources other than dark clouds C_4H and C_6H were detected in only two (the translucent cloud CB17 and the carbon star CRL2688), and C_6H^- was not detected in any. In CB17, R_N is about 1% and $R_A < 4\%$, similar to that in dark clouds. The upper limit of R_A in CRL2688 (23%) is nearly three times larger than that found in IRC+10216 (8.6%; Kasai et al. 2007). The three species were not detected in the Horsehead nebula, where C_4H and C_6H have previously been reported in the 3 mm wave band (Teyssier et al. 2004; Agúndez et al. 2008).

4. DISCUSSION

As might be expected from the close structural similarity, the column densities of C_6H and C_4H in cold dark clouds are closely correlated. A similar correlation between the cyanopolyynes HC_3N and HC_5N, and between C_4H and cyanopolyynes was previously observed by Federman et al. (1990), who concluded that long carbon chains are probably formed by similar processes. There have been several published chemical model calculations of carbon chain abundances in TMC-1—the cold dark cloud that has received the most observational and theoretical attention. In a recent time-dependent model optimized for TMC-1 (Millar et al. 2007), the column densities of C_6H and C_4H are

Table 4
Lines Observed Toward L1544 and L1521F

Transition $F' - F$	T_A (mK)	v_{LSR} (km s^{-1})	Δv (km s^{-1})	$\int T_A dv$ (K km s^{-1})
L1544				
C_4H				
($J = 2.5 - 1.5$)				
$2 - 1$	209(3)	7.09(3)	0.18(3)	0.11(2)
	453(4)	7.34(3)	0.15(3)	···
$3 - 2$	310(3)	7.10(3)	0.20(3)	0.18(3)
	678(4)	7.35(3)	0.15(3)	···
$2 - 2$	27(2)	7.08(4)	0.22(3)	0.015(3)
	60(2)	7.34(4)	0.14(1)	···
($J = 1.5 - 0.5$)				
$1 - 1$	44(3)	7.09(4)	0.19(3)	0.019(3)
	71(3)	7.37(3)	0.15(1)	···
$2 - 1$	200(3)	7.09(3)	0.20(3)	0.12(2)
	435(4)	7.34(3)	0.15(1)	···
$3 - 2$	93(3)	7.07(4)	0.19(3)	0.045(7)
	175(4)	7.34(3)	0.15(1)	···
C_6H				
$7 - 6, e$	42(3)	7.03(3)	0.21(2)	0.028(3)
	113(3)	7.32(3)	0.16(2)	···
$6 - 5, e$	49(3)	7.07(3)	0.18(14)	0.023(3)
	95(3)	7.34(3)	0.14(1)	···
$7 - 6, f$	48(4)	7.07(3)	0.15(1)	0.025(3)
	114(4)	7.36(4)	0.14(2)	···
$6 - 5, f$	41(4)	7.05(4)	0.30(4)	0.025(3)
	88(4)	7.30(3)	0.13(1)	···
C_6H^-				
	16(2)	7.08(3)	0.16(3)	0.0060(12)
	26(2)	7.30(3)	0.13(3)	···
L1521F				
C_4H				
($J = 2.5 - 1.5$)				
$2 - 1$	209(3)	6.38(3)	0.25(3)	0.11(1)
	453(4)	6.60(3)	0.21(3)	···
$3 - 2$	506(5)	6.39(3)	0.26(3)	0.17(2)
	148(8)	6.63(3)	0.21(3)	···
$2 - 2$	52(3)	6.38(4)	0.29(3)	0.018(2)
	12(3)	6.65(5)	0.15(8)	···
($J = 1.5 - 0.5$)				
$1 - 1$	108(8)	6.32(3)	0.28(3)	0.040(5)
	55(7)	6.54(5)	0.22(5)	···
$2 - 1$	305(4)	6.39(3)	0.28(3)	0.11(1)
	72(3)	6.63(3)	0.19(3)	···
$3 - 2$	66(3)	6.38(3)	0.20(4)	0.019(1)
	26(4)	6.63(6)	0.15(8)	···
C_6H				
$7 - 6, e$	58(3)	6.34(3)	0.30(2)	0.020(3)
	14(3)	6.59(5)	0.13(2)	···
$6 - 5, e$	44(3)	6.30(3)	0.23(4)	0.016(3)
	25(3)	6.55(3)	0.22(3)	···
$7 - 6, f$	53(4)	6.38(4)	0.24(1)	0.015(3)
	10(4)	6.64(4)	0.15(2)	···
$6 - 5, f$	37(4)	6.27(5)	0.30(4)	0.011(3)
	13(4)	6.33(5)	0.13(1)	···
C_6H^-				
	17(2)	6.33(5)	0.18(3)	0.007(1)
	9(2)	6.64(5)	0.35(9)	···

Notes. Rest frequencies in MHz (see Gottlieb et al. 1983; McCarthy et al. 1999, 2006). C_6H^- ($J = 7 - 6$): 19276.038(2) MHz; C_4H ($N, J = 2, 2.5 - 1, 1.5$): 19014.720(2) ($F = 2 - 1$), 19015.144(2) ($3 - 2$), and 19025.107(4) ($2 - 2$); C_4H ($N, J = 2, 1.5 - 1, 0.5$): 19044.760(5) ($1 - 1$), 19054.476(2) ($2 - 1$), and 19055.947(2) ($3 - 2$); C_6H ($^2\Pi_{3/2}$, $J = 6.5 - 5.5$): 18020.574(2) ($F = 7 - 6$, Λ-component e), 18020.644(1) ($6 - 5, e$), 18021.752(4) ($7 - 6, f$), and 18021.818(1) ($6 - 5, f$). Line parameters derived from least-squares fit of two Gaussian profiles to spectra shown in Figures 3 and 4.

Table 5
Column Densities and Abundance Ratios

Source	T_{rot}^a (K)	$N(C_4H)$ (10^{13} cm^{-2})	$N(C_6H)$ (10^{11} cm^{-2})	$N(C_6H^-)$ (10^9 cm^{-2})	R_N (%)	R_A (%)
L1544	10	18(6)	12(3)	31(5)	0.7(2)	2.5(8)
L1521F	10	17(3)	8(1)	34(7)	0.45(6)	4(1)
L1512	10	9(3)	5(2)	< 48	0.5(2)	< 11
L1521B	10	10(2)	8(3)	< 17	0.8(3)	< 2.2
L1495B	10	15(5)	13(1)	< 310	0.9(1)	< 2.4
L183	10	3(2)	< 4.3	< 120	< 0.39	···
Barnard 1	10	7(6)	< 1.3	< 97	< 0.18	···
L1521E	10	7(3)	< 2.7	< 66	< 0.39	···
IRAM04191+1522	10	3(1)	< 2.3	< 52	< 0.70	···
L1082A	10	2(1)	< 1.5	< 48	< 0.71	···
L1551	10	< 4	< 3.2	< 98	< 0.82	···
L1251	10	5(3)	< 3.7	< 190	< 0.69	···
CB17(L1389)	10	5(2)	6(3)	< 25	1.2(8)	< 4.2
B0415+379 (3C111)	30	< 3	< 9	< 9	···	···
Horsehead Nebula	15	< 2	< 250	< 4.3	···	···
NGC1333-2A	50	< 1.2	< 39	< 1300	···	···
NGC1333-4A	50	< 1	< 44	< 1200	···	···
W3(HCN)	30	< 4.1	< 18	< 600	···	···
SgrB2N	30		< 2600	···	···	···
W51 M/S	30		< 2200	···	···	···
CRL618	90	< 33	< 140	< 4000	···	···
CIT6	13	< 18	< 56	< 2800	···	···
CRL2688	25	35(4)	45(1)	< 1000	1.3(2)	< 23
CRL3068	17	< 8	< 40	< 1700	···	···

Notes. Column densities were calculated (see Cummins et al. 1986) from the velocity integrated intensities ($\int T_A dv$) in Tables 3 and 4, and corrected for beam efficiencies given in Table 1. Assumed dipole moments: 8.2 D for C_6H^- (Blanksby et al. 2001); 0.9 D for C_4H; and 5.5 D for C_6H (Woon 1995).
[a] Assumed rotational temperature (see references in Table 2).

too low by a factor of 3 and 13, respectively, and R_N is too low by a factor of 4. Better agreement for the calculated R_N could be attained at longer assumed times (i.e., $> 3.16 \times 10^5$ yr), but the column densities would then be much too low. Owing to uncertainties in the calculated abundances of C_4H and C_6H, it is premature to infer the ages of dark clouds and to make detailed comparisons of the chemistry of different clouds on the basis of current time-dependent chemical models and the measurements reported here.

The calculated abundances of anions are even more uncertain than those of the corresponding neutral species, because as noted by Millar et al. (2007) the rates for radiative electron attachment ($A + e \rightarrow A^- + h\nu$), and the product distributions (branching ratios) of subsequent reactions of molecular anions with atomic species have not been measured in the laboratory. Although the calculated R_A for TMC-1 is only about three times higher than that observed (Brünken et al. 2007), the calculated C_4H^-/C_4H ratio is at least 10–100 times too high (Thaddeus et al. 2008; Herbst & Osamura 2008). A detailed quantitative comparison of the calculated abundances of C_4H, C_6H, and C_6H^- with those in Table 5, awaits laboratory measurements of the rates of formation and destruction of these carbon chain radicals and anions.

The C_6H^- anion may be close to detection in at least three other dark clouds included here. The R_A in TMC-1, L1544, and L1521F is similar (Figure 1(c)), indicating that C_6H^- might be detectable in clouds where the column density of C_6H [$N(C_6H)$] is comparable to these representative sources. In three clouds (L1521B, L1495B, and L1512), R_N and $N(C_6H)$ are comparable to those in L1544 and L1521F (Figure 1 and Table 5). For

example, in L1521B the upper limit of $N(C_6H^-)$ (corresponding to $R_A \sim 2\%$) is at least a factor of 3 lower than the other dark clouds in Table 5, suggesting that C_6H^- may be detectable in a few other sources (especially L1495B and L1512) with only 3 to 4 times deeper integration. If sources with R_A comparable to that of L1527 are found (∼10%; Sakai et al. 2007), then C_6H^- might be detectable even if lines of C_6H are weak.

Detection of C_6H^- toward other sources should be possible with deeper searches. Lines of C_6H in CRL2688 near 20 GHz are fairly weak (< 5 mK), so detection of the anion in this frequency band would require a ninefold deeper integration if R_A is comparable to that in IRC+10216. Because CRL2688 is a fairly warm source ($25 < T_{\rm rot} < 80$ K), searches for transitions in the millimeter-wave band from levels near the peak of the Boltzmann distribution might yield detection of C_6H^-. In CB17, our upper limit for R_A of 4% is only slightly greater than that observed in dark clouds, but lines of C_6H are quite weak (∼ 20 mK; see Table 3). If R_A is similar to that for the three representative dark clouds (L1544, L1521F, and TMC-1), then C_6H^- might be detectable in CB17 with 40–50 hr of integration.

The fairly narrow range of R_A (Figure 1(c)) might reflect differences in the rate of production of C_6H^- in the four known dark clouds. Because the electron abundance varies as $n^{1/2}$, whereas the H abundance is predicted to be independent of the density (Li & Goldsmith 2003; Flower et al. 2007), the observed variation in R_A may reflect differences in the electron abundances in these sources. In L1544, L1521F, and TMC-1 ($n \sim 10^4$–10^5 cm^{-3}) R_A is 1%–4%, while in L1527 ($n \sim 10^6$ cm^{-3}) R_A is 3 to 5 times higher, consistent with the higher estimated density (Sakai et al. 2007; see Appendix).

The anion-to-neutral ratio may yield a fairly direct measure of the electron density in dark clouds. We illustrate this by an approximate calculation of e/H_2 from the observed R_A, the rate of electron attachment (k_{ra}) to C_6H, and the abundance of atomic hydrogen (see Appendix). For L1544 and L1521F, our estimate of the fractional ionization from a single point measurement of 10^{-8} to 10^{-7}, is somewhat higher than that obtained from extensive measurements and analysis of N_2D^+ and N_2H^+ (Caselli et al. 2002b; Crapsi et al. 2004), but closer to that derived from observations of CO, HCO^+, and DCO^+ toward low-mass cores. The two main sources of uncertainty are k_{ra}, and the abundance of H. Laboratory measurements of k_{ra} as well as possible improved estimates of the H abundance in dark clouds (e.g., Goldsmith et al. 2007) may allow tighter constraints on the fractional ionization derived from molecular anions.

5. CONCLUSIONS

This survey has resulted in an increase in the number of known galactic sources of C_4H by nearly 50%, and C_6H by more than twofold. Although relatively few molecular clouds have been surveyed for large carbon chain radicals, our results for dark clouds indicate that the abundance of C_6H may be closely tied to that of C_4H. Here, C_4H was observed in nearly all dark clouds, and C_6H in those which showed strong lines of C_4H, indicating that C_4H may be a useful surrogate for large carbon chains in future surveys.

The two new sources of C_6H^- found here increase the number of sources accessible to the study of molecular anions by nearly twofold, and more may be found in similar surveys. Some promising sources yet to be studied include dark clouds in the Aquila rift, e.g., L492, where large cyanopolyynes are as abundant as in TMC-1 (Hirota & Yamamoto 2006), and the carbon star IRAS 15194-5115, where C_4H is three times more abundant than in IRC+10216 (Nyman et al. 1993).

The results here suggest that molecular anions may be close to detection in many astronomical sources—in dark clouds especially, but in other sources as well. At present C_6H^- is the best available probe of the negative charge (see Appendix), but that may change with the discovery of other molecular anions. Of the more than 1000 molecular anions that have been investigated in the laboratory (Rienstra-Kiracofe et al. 2002), so far only linear carbon chains and two simple diatomics (OH^- and SH^-; Matsushima et al. 2006; Civiš et al. 1998) have been studied at the high resolution required for radio astronomical searches. Laboratory detection of other types of anions whose parent molecules are widely distributed should extend the study of molecular anions to sources deficient in carbon chains, and mark a significant advance in the search for new sources of molecular anions.

We are indebted to P. C. Myers for many helpful discussions and suggestions during the course of this survey. We are grateful for helpful suggestions from T. L. Bourke, S. Brünken, A. Dalgarno, N. J. Evans II, J. F. Stanton, and W. Klemperer. It is a pleasure to acknowledge useful conversations with A. J. Remijan, particularly with respect to the Green Bank Telescope. This work is supported by the National Science Foundation (NSF) grant CHE-0701204 and NASA grant NNX08AE05G; support for H.G. was provided by the NSF through grant CHE-0710146 to Stanton at the University of Texas and award GSSP-07A-0100 from the NRAO.

APPENDIX

ESTIMATES OF FRACTIONAL IONIZATION FROM MOLECULAR ANIONS

Molecular anions provide an independent means of estimating the fractional ionization ($x_e \equiv [e]/[H_2]$) of molecular clouds (see e.g., Flower et al. 2007). So far, x_e has mainly been estimated indirectly from observations of molecular cations in conjunction with chemical models, but large uncertainties remain in its determination (for a review, see Caselli 2002d). The most reliable estimate of x_e might be obtained from a simultaneous analysis of the measured abundances of anions and cations based on the assumption that they are codistributed in the cloud.

The formation of C_6H^- likely occurs via radiative attachment

$$C_6H + e \xrightarrow{k_{ra}} C_6H^- + h\nu, \tag{A1}$$

and its destruction by neutralization with positive ions and associative detachment with atomic hydrogen

$$C_6H^- + M^+ \xrightarrow{k_{neu}} C_6H + M, \tag{A2}$$

$$C_6H^- + H \xrightarrow{k_{ad}} HC_6H + e, \tag{A3}$$

where M^+ is any positive ion. We neglect dissociative attachment to the carbene C_6H_2 as a route to the formation of C_6H^-, and charge transfer (to large molecules or grains) and photodetachment as routes to the destruction of C_6H^- (see e.g., Sakai et al. 2007 and Agúndez et al. 2008). At steady state,

$$\frac{[C_6H^-]}{[C_6H]} = \frac{k_{ra}[e]}{(k_{neu}[M^+] + k_{ad}[H])}, \tag{A4}$$

where $[e]$ is the abundance of electrons, $[M^+]$ that of cations, and [H] that of atomic hydrogen. We adopt $k_{ra} = 5 \times 10^{-8}$ cm^3s^{-1} obtained from observations toward two quite different sources (IRC+10216 and L1527; Cernicharo et al. 2007; Sakai et al. 2007); $k_{ad} = 5 \times 10^{-10}$ cm^3s^{-1} was accurately determined from laboratory measurements (Barckholtz et al. 2001). On the assumption that reaction (A3) is the dominant loss mechanism of C_6H^- at densities $< 10^6$ cm^{-3} (Sakai et al. 2007), Equation (A4) reduces to

$$\frac{[C_6H^-]}{[C_6H]} \sim \frac{k_{ra}[e]}{k_{ad}[H]}. \quad \text{(A5)}$$

In L1544 and L1521F, the gas densities are estimated to lie between 10^4 and 10^5 cm^{-3} except in the dense cores (Caselli et al. 2002b; Crapsi et al. 2004). From Equation (A5), $[e]/[H]$ is 2.5×10^{-4} for L1544 and 4×10^{-4} for L1521F. Adopting $[H]/[H_2] = 1 \times 10^{-3}$ cm^{-3} (Li & Goldsmith 2003), our estimate of $x_e = 10^{-8}$ to 10^{-7} is somewhat higher than that from earlier measurements of N_2D^+/N_2H^+ (Caselli et al. 2002b; Crapsi et al. 2004), but close to that obtained from observations of CO, HCO^+, and DCO^+ in dense cores (Caselli et al. 1998; Williams et al. 1998).

REFERENCES

Agúndez, M., Cernicharo, J., Guélin, M., Gerin, M., McCarthy, M. C., & Thaddeus, P. 2008, A&A, 478, L19
Bachiller, R., Menten, K. M., & del Río-Alvarez, S. 1990, A&A, 236, 461
Barckholtz, C., Snow, T. P., & Bierbaum, V. M. 2001, ApJ, 547, L171
Belloche, A., André, P., Despois, D., & Blinder, S. 2002, A&A, 393, 927
Blanksby, S. J., McAnoy, A. M., Dua, S., & Bowie, J. H. 2001, MNRAS, 328, 89
Bourke, T. L., et al. 2006, ApJ, 649, L37
Brünken, S., Gupta, H., Gottlieb, C. A., McCarthy, M. C., & Thaddeus, P. 2007, ApJ, 664, L43
Buckle, J. V., Rodgers, S. D., Wirstrom, E. S., Charnley, S. B., Markwick-Kemper, A. J., Butner, H. M., & Takakuwa, S. 2006, Faraday Discuss., 133, 63
Caselli, P. 2002d, Planet. Space Sci., 50, 1133
Caselli, P., Benson, P. J., Myers, P. C., & Tafalla, M. 2002a, ApJ, 572, 238
Caselli, P., Walmsley, C. M., Terzieva, R., & Herbst, E. 1998, ApJ, 499, 234
Caselli, P., Walmsley, C. M., Zucconi, A., Tafalla, M., & Myers, P. C. 2002b, ApJ, 565, 331
Caselli, P., Walmsley, C. M., Zucconi, A., Tafalla, M., & Myers, P. C. 2002c, ApJ, 565, 344
Cernicharo, J., Guélin, M., Agúndez, M., Kawaguchi, K., McCarthy, M. C., & Thaddeus, P. 2007, A&A, 467, L37
Civiš, S., Walters, A., Tretyakov, M.-Y., Bailleux, S., & Bogey, M. 1998, J. Chem. Phys., 108, 8369
Codella, C., Welser, R., Henkel, C., Benson, P. J., & Myers, P. C. 1997, A&A, 324, 203
Cox, P., Güsten, R., & Henkel, C. 1988, A&A, 206, 108
Crapsi, A., Caselli, P., Walmsley, C. M., Tafalla, M., Lee, C. W., Bourke, T. L., & Myers, P. C. 2004, A&A, 420, 957
Crapsi, A., Caselli, P., Walmsley, C.M., Myers, P. C., Tafalla, M., Lee, C. W., & Bourke, T. L. 2005, ApJ, 619, 379
Cummins, S. E., Linke, R. A., & Thaddeus, P. 1986, ApJS, 60, 819
Dalgarno, A., & McCray, R. A. 1973, ApJ, 181, 95
Douglas, A. E., & Herzberg, G. 1941, ApJ, 94, 381
Federman, S. R., Huntress, W. T., Jr., & Prasad, S. S. 1990, ApJ, 354, 504
Flower, D. R, Pineau des Forêts, G., & Walmsley, C. M. 2007, A&A, 474, 923
Fukasaku, S., Hirahara, Y., Masuda, A., Kawaguchi, K., Ishikawa, S., Kaifu, N., & Irvine, W. M. 1994, ApJ, 437, 410
Fuller, G. A., & Myers, P. C. 1993, ApJ, 418, 273
Goldsmith, P. F., Li., D., & Krco, M. 2007, ApJ, 654, 273
Gottlieb, C. A., Gottlieb, E. W., Thaddeus, P., & Kawamura, H. 1983, ApJ, 275, 916
Herbst, E. 1981, Nature, 289, 656
Herbst, E., & Osamura, Y. 2008, ApJ, 679, 1670
Highberger, J. L., Savage, C., Bieging, J. H., & Ziurys, L. M. 2001, ApJ, 562, 790
Highberger, J. L., Thomson, K. J., Young, P. A., Arnett, D., & Ziurys, L. M. 2003, ApJ, 593, 393
Hirota, T., Ito, T., & Yamamoto, S. 2002, ApJ, 565, 359
Hirota, T., Maezawa, H., & Yamamoto, S. 2004, ApJ, 617, 399
Hirota, T., & Yamamoto, S. 2006, ApJ, 646, 258
Jörgensen, J. K., Bourke, T. L., Myers, P. C., Schöier, F. L., van Dischoeck, E. F., & Wilner, D. J. 2005, ApJ, 632, 973
Kasai, Y., Kagi, E., & Kawaguchi, K. 2007, ApJ, 661, L61
Kawaguchi, K., et al. 2007, PASJ, 59, L47
Lefloch, B., Castets, A., Cernicharo, J., Langer, W. D., & Zylka, R. 1998, A&A, 334, 269
Li, D., & Goldsmith, P. F. 2003, ApJ, 585, 823
Lucas, R., & Liszt, H. S. 2000, A&A, 358, 1069
Madden, S. C., Irvine, W. M., Matthew, H., Friberg, P., & Swade, D. A. 1989, AJ, 97, 1403
Matsushima, F., Yonezu, T., Okabe, T., Tomaru, K., & Moriwaki, Y. 2006, J. Mol. Spectrosc., 235, 261
McCarthy, M. C., Chen, W., Apponi, A. J., Gottlieb, C. A., & Thaddeus, P. 1999, ApJ, 520, 158
McCarthy, M. C., Gottlieb, C. A., Gupta, H., & Thaddeus, P. 2006, ApJ, 652, L141
Millar, T. J., Walsh, C., Cordiner, M. A., Ní Chuimín, R., & Herbst, E. 2007, ApJ, 662, L87
Morris, M., Turner, B. E., Palmer, P., & Zuckerman, B. 1976, ApJ, 205, 82
Nyman, L.-Å., Olofsson, H., Johansson, L. E. B., Booth, R. S., Carlström, U., & Wolstencroft, R. 1993, A&A, 269, 377
Ohashi, N., Lee, S., Wilner, D. J., & Hayashi, M. 1999, ApJ, 518, L41
Remijan, A. J., Hollis, J. M., Lovas, F. J., Cordiner, M. A., & Millar, T. J. 2007, ApJ, 664, L47
Rienstra-Kiracofe, J. C., Tschumper, G. S., Shaeffer, H. F., III, Nandi, S., & Ellison, G. B. 2002, Chem. Rev., 102, 231
Sakai, N., Sakai, T, Hirota, T., & Yamamoto, S. 2008, ApJ, 672, 371
Sakai, N., Sakai, T, Osamura, Y., & Yamamoto, S. 2007, ApJ, 667, L65
Sarre, P. J. 1980, J. Chim. Phys. Phys.-Chim. Biol., 77, 769
Tafalla, M., Mardones, D., Myers, P. C., Caselli, P., Bachiller, R., & Benson, P. J. 1998, ApJ, 504, 900
Teyssier, D., Fossé, D., Gerin, M., Pety, J., Abergel, A., & Roueff, E. 2004, A&A, 417, 135
Thaddeus, P., Gottlieb, C. A., Gupta, H., Brünken, S., McCarthy, M. C., Agúndez, M., Guélin, M., & Cernicharo, J. 2008, ApJ, 677, 1132
Turner, B. E. 1994, ApJ, 420, 661
Turner, B. E., & Thaddeus, P. 1977, ApJ, 211, 755
Williams, J. P., Bergin, E. A., Caselli, P., Myers, P. C., & Plume, R. 1998, ApJ, 503, 689
Womack, M., Ziurys, L. M., & Wyckoff, S. 1992, ApJ, 387, 417
Woon, D. E. 1995, Chem. Phys. Lett, 244, 45